Canadian Conference - Pacific Conference on Earthquake Engineering 2023
Vancouver, British Columbia
June 25th – June 30th, 2023

Effects of modeling of the welded vertical inter-module connection on the nonlinear dynamic response of a low-rise modular steel building

Mehmet Baris Batukan[1*] and Oya Mercan[2]

[1]PhD Student, Department of Civil and Mineral Engineering, University of Toronto, Toronto, ON, Canada
[2]Professor, Department of Civil and Mineral Engineering, University of Toronto, Toronto, ON, Canada
[*]mehmet.batukan@mail.utoronto.ca (Corresponding Author)

ABSTRACT

Modular steel buildings (MSB) are now recognized as a rapid solution to address urgent housing needs across the globe. Volumetric MSBs consist of prefinished 3-D modules produced off-site and assembled on-site to form a permanent building. Depending on the structural mechanism, continuously- or corner-supported modules can be used to transfer the loads all the way to the foundation. When the latter is selected, diaphragm action and inter-module connections play a crucial role and may cause considerable differences in the nonlinear dynamic performance of MSBs. Despite the availability of various connection options and proposed alternatives as research on MSBs continues, on-site welding remains one of the methods used for vertical connectivity between the modules. This paper offers a comparative analysis aimed at identifying the effects of various welded connection models on the overall nonlinear dynamic response. For this purpose, two existing models of welded vertical inter-module connection (VC1 and VC2) from the literature, both were calibrated using experimental data, were selected and studied on a 4-story MSB. In order to obtain the parameters of VC2, detailed finite element analyses were carried out using Ansys software. Consequently, two different 3-D global models were developed using OpenSees to investigate the system-level nonlinear dynamic response of the selected building under bidirectional ground shaking. In addition, the base shear values, inter-story drift ratios, and hinge formation sequences of structural elements were investigated and compared between the two global models with different inter-module connection models to shed light on the dynamic performance of the building subjected to bidirectional ground shaking. The results show that the simpler model (VC1) does not cause dramatic differences in the nonlinear dynamic response of the low-rise MSB, even though it slightly overestimates the lateral response of the inter-module connection.

Keywords: Modular Steel Building, Nonlinear Dynamic Analysis, Numerical Analysis, Seismic Response, Inter-module Connection.

INTRODUCTION

Modular construction of volumetric modular buildings involves manufacturing 3-D modules off-site in a controlled environment, which are then transported to the construction site for assembly of the permanent structure [1]. Volumetric modular buildings are becoming increasingly popular thanks to their many advantages, such as faster construction time, higher quality control, and reduced disruption to the local community while the construction work is underway [1].

Volumetric modular buildings are made of continuously- and corner-supported modules. Corner-supported modules use edge beams that span between corner columns to provide structural support. Conversely, continuously-supported modules utilize load-bearing walls that offer continuous support [2]. In recent years, studies on the structural response of corner-supported multi-story modular steel buildings (MSBs) have shown that the lateral behavior of these structures differs from that of traditional steel buildings. For instance, Annan et al. [3] experimentally tested a modular steel-braced frame with a welded vertical connection and compared it with a counterpart. As a result, it was reported that special detailing requirements, such as vertical inter-module connections, should be incorporated in the design and modeling of MSBs. Moreover, Fathieh and Mercan studied the seismic behavior of a 4-story MSB having corner-supported modules and welded vertical inter-module connections. They concluded that inelasticity is concentrated at the first level of the building, and separate diaphragms play a crucial role in the lateral stiffness and drifts of the building [4].

Although on-site welding is one of the methods used for vertical connectivity, several connection types, such as bolted and post-tensioned connections, have been studied for MSBs [5]. For example, Lacey et at. [6] studied the effect of the bolted inter-module connection on the lateral response of a 6-story MSB. It was shown that connection stiffness changes the overall response to the wind and earthquake loads. Sanches et al. [7] experimentally tested a subassembly with a post-tensioned connection for vertical connectivity. Later, Sanches [8] reported that the post-tensioned connection could improve the building's performance. Srisangeerthanan et al. [5] mentioned that inter-module connections are expected to have a significant impact since they affect the assembly of modules on-site during the construction of successive stories.

Past research suggests that how modules are connected is a crucial factor affecting the lateral response of MSBs. Therefore, this paper provides a study that compares different welded connection models and their impacts on the nonlinear dynamic response of MSBs. For the study, two different models of welded vertical inter-module connections from the literature, both of which were calibrated with experimental data, were selected and analyzed on a 4-story MSB. First, the parameters of one of the connection models were obtained through detailed finite element (FE) analyses conducted using Ansys [9]. Next, two different 3-D global models were developed using Open System for Earthquake Engineering Simulation (OpenSees) [10] to explore the system-level nonlinear dynamic response of the selected building under bidirectional ground shaking. Finally, to gain insight into the dynamic behavior of the system, transient and residual inter-story drift ratios, hinge formation sequences of structural elements, and base shear values were analyzed and compared between the two global models with different inter-module connection models.

NUMERICAL MODELLING

A 4-story MSB from the literature was chosen to investigate the effects of welded vertical connection on a low-rise MSB. The selected building was previously designed by Fathieh and Mercan [4] in accordance with the National Building Code of Canada (NBCC) [10] to assess its nonlinear seismic performance. As shown in Figs. 1a, b, and c, the building's seismic force resisting system (SFRS) comprises concentrically braced frames (CBFs) in both directions. The building's total height is 13.75 m, and the total area is about 191 m^2. While centerline to centerline horizontal distance between modules is 0.35 m, the vertical distance is 0.25 m which leaves about a 0.15 m gap to accommodate mechanical and electrical facilities. A typical floor system comprising concrete floor, insulation, and steel deck is preferred for the building. According to the NBCC, the live loads of 1.9, 4.8, and 1.0 kPa are applied to the rooms, corridors, and roof, respectively. Additionally, superimposed dead loads of 0.7, 0.75, and 0.32 kPa are considered for ceiling, floor, and roof levels, respectively. In order to investigate the effects of modeling the welded vertical inter-module connection, two global models were developed on OpenSees. Details of the global models are explained in the following sections.

Description of main components

Beam and columns

In the MSB, each story has 12 corner-supported modules and 24 bays in both directions. Four (floor and ceiling) beams are located at each module. While the beams are made of wide sections (W), square hollow structural sections (HSS) are used for columns. Table 1 shows all the beam and column sections. Concentrated plasticity modeling is used for all the beams and columns to incorporate nonlinearity in the numerical model. For this reason, the elasticBeamColumn element and the zeroLength element from OpenSees library represent all the beams and columns. Except for the first-floor columns, every beam and column have two nonlinear hinges at their ends. The first-floor columns have only one nonlinear hinge at the top because they are pinned at the base. Force-deformation relationship of the beam hinges is obtained from the component model created by Lignos and Krawinkler [12], where the component model was calibrated using more than 300 specimens. For the columns made of HSS, another component model [13], which accounts for an axial load on deterioration parameters, is used to find hinge parameters. W sections are assumed to be produced to ASTM A992 grade 50 (F_y = 345 MPa), whereas HSS is manufactured to CSA G40.20 Standard (F_y = 350 MPa).

Table 1. Member Section of the MSB.

Story	Floor Beam	Ceiling Beam	Column	Brace
1	W100x19	W100x19	HS127x127x4.8	HS76x76x4.8
2	W100x19	W100x19	HS102x102x6.4	HS76x76x4.8
3	W100x19	W100x19	HS102x102x6.4	HS51x51x4.8
4	W100x19	W100x19	HS76x76x4.8	HS51x51x4.8

Braces

The CBFs (See Figs. 1a and b) have X-type of tension-compression diagonal bracing members. While only one bay in the X-direction has braces, two bays are equipped with diagonal braces in the Y-direction. Similar to the columns, bracing members

are made of square HSS, also listed in Table 1. The diagonal braces in the MSB are subjected to substantial cyclic deformations when subjected to intense vibrations or lateral movements. During the tension-yielding phase, the brace deforms inelastically through axial deformation. Plastic rotations of the flexural plastic hinges occur in compression as the brace inelastically buckles. While there are a few alternative ways in the literature to model the nonlinear behavior of the brace, the model by Hsiao et al. [14] is chosen for this study.

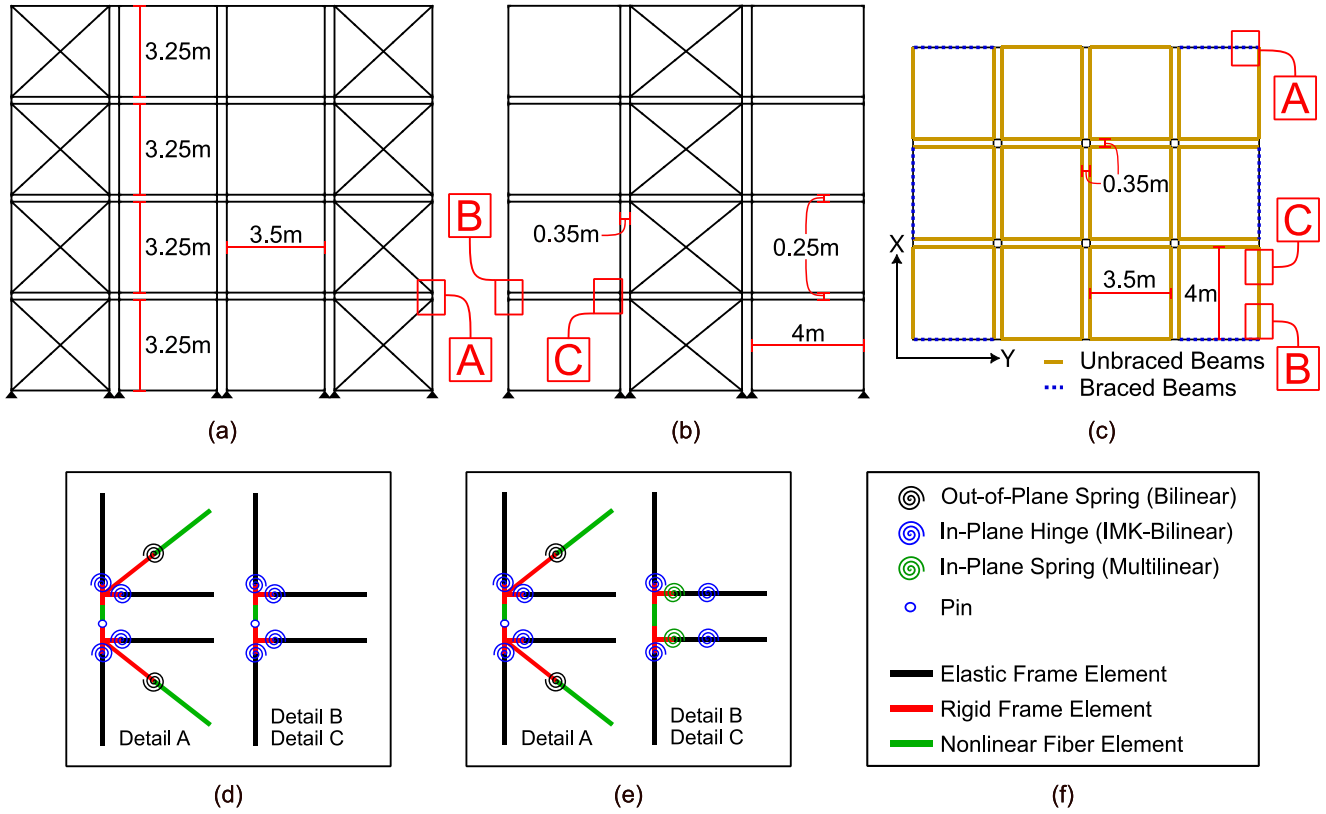

Figure 1. Details of the numerical model of the MSB: (a) braced frame in Y-direction, (b) braced frame in X-direction, (c) plan view, (d) vertical connection details of Model 1, (e) vertical connection details of Model 2, (f) legend of the d and e.

In the selected model, brace elements are divided into three segments. The first and last segments are rigid portions of the brace element, which connect the middle segment to the column and beam with a gusset plate. The middle segment is a nonlinear portion subjected to axial and flexural deformations. Therefore, it is modeled with a nonlinear dispBeamColumn element on OpenSees. As suggested by Hsiao et al. [14], the middle segment is discretized into ten subsegments having out-of-plane imperfection of 0.2% of the length of the brace.

Furthermore, the cross-section of the middle segment is discretized using four and ten fibers along the thickness and width of a brace, respectively. UniaxialMaterial (Steel02) is chosen for the fiber section with a yield stress of 350 MPa and a strain-hardening ratio of 0.01. Gauss-Lobatto integration with five integration points along the length of the element is used for the middle segment. Because excessive geometric nonlinearity is expected in braces, the corotational coordinate transformation is assigned to these elements. Additionally, bilinear rotational springs at both ends of the middle segment represent out-of-plane deformation at the brace and gusset plate intersection. The yield moment and strain-hardening ratio of the spring material (Steel01) depend on the geometric and material properties of the gusset plate. Thus, it is assumed that the gusset plate is 200 mm long with a thickness of 16 mm and yield stress of 300 MPa. It should be noted that fracture in the brace element is not considered and is out of the scope of this study.

Connections

There are three types of connections in the MSB: (i) foundation-to-module, (ii) intra-module, and (iii) inter-module. Foundation-to-module connections at the base of the building transfer loads to the foundation. A pin connection at the base was used for foundation-to-module connections [4]. Therefore, moments of the base nodes are released in the model. Second, intra-module connections connect stringers to the beams and the beams to the columns. It is anticipated that the connections within

each module would ensure its structural integrity and help attain the necessary stiffness of the module [5]. Additionally, they transfer lateral loads if they are part of SFRS. The stringer-to-beam connections transfer the floor and ceiling loads to the beams. They are assumed to be rigid connections and part of the rigid diaphragm of every module. Therefore, they are not included in the numerical model. There are 96 beam-column connections at every story, and 24 are part of the SFRS. The remaining 72 connections are mainly designed to transfer gravity loads. They can, however, contribute to the lateral stiffness of the building and transfer lateral loads to the foundation depending on the intra- and inter-module connections. Third, inter-module connections provide connectivity between modules in the vertical and horizontal directions so that the loads can be transferred between modules. It is assumed that every module is horizontally bolted to the other module at their corners, and these connections are designed to remain elastic [4]. An elasticBeamColumn element having 30% higher shear and bending capacity than adjacent beams is used for horizontal connection (HC).

The vertical inter-module connections of the building were designed to be welded on-site [4]. This study utilizes two experimental studies from the literature pertaining to this type of connection. The first model (VC1) was calibrated using a dataset for a welded vertical inter-module connection from a modular braced frame by Annan et al. [3]. The schematic representation of the VC1 is shown in Fig. 1d. Modules are connected with a nonlinear element, and the moment at the lower end is released to capture independent rotations at the same joint [3]. A dispBeamColumn element with Gauss-Lobatto integration is used to incorporate the VC1 into the global model.

The second model (VC2) was proposed by Sanches [8]. They tested a full-scale subassembly from an unbraced modular frame [7]. It was observed that nonlinearity is concentrated on the intra-module connections (beam ends), and the connection showed a semi-rigid behavior rather than fully rigid. A simplified model of the VC2 was developed to facilitate system-level analysis, and it is shown in Fig. 1e. In the simplified model, a continuous column between modules provides vertical inter-module connectivity, and a spring was added to the intra-module connections to account for softening in the connection region. In both models, the rigid elements were defined to include rigidity in the connection area due to the depth of beams and columns.

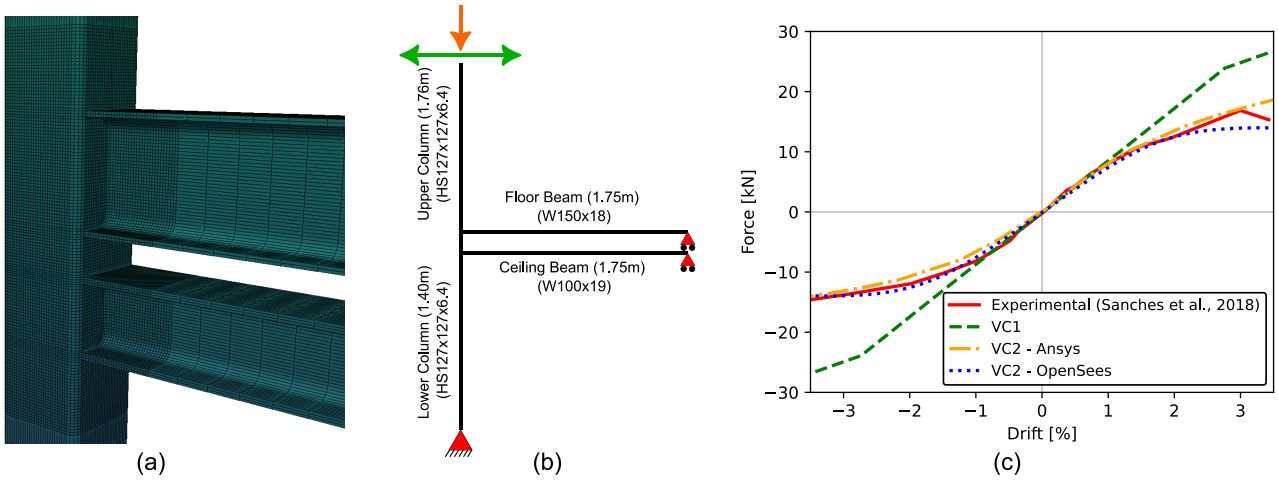

Figure 2. Details of the subassembly: (a) close-up view of the Ansys model, (b) schematic representation, (c) backbone curves.

The moment-rotation relationship of the spring element in the VC2 was defined using the three-parameter power model [15], expressed in Eq. (1). To calibrate the spring parameters, it is recommended to use either an experimental dataset or a FE model. For this study, a numerical model was developed to calibrate the spring parameters. Before the calibration process, the FE model was validated against the experimental dataset. For this purpose, a detailed FE model of a subassembly from Sanches et al. [7] was modeled using Ansys [16]. The schematic representation of the FE model is shown in Fig. 2b. The columns and beams are made of HSS and W-sections, respectively. The 3-D FE model (See Fig. 2a) was created with 8-node solid elements (SOLID-185) from Ansys's element library. To accurately capture the response, 6 mm fillet welds around beam-column connections were also included in the model. As suggested by Bu [17], a gap of 0.25 mm is left between the beam and column surfaces to allow loads to flow only through the welds. The weld between the upper and lower columns was not separately modeled, as the column in VC2 is assumed to be continuous. A bilinear material was assigned to each element, and material properties can be found in Ref. [7]. Finer mesh was chosen for the regions where high nonlinearity is expected. A coarser mesh was preferred for the rest of the model to reduce computational cost and time. There are more than 250K elements and 300K nodes in the FE model. Boundary conditions shown in Fig. 2b were applied to the FE model. A pivot node was defined to represent a pin-joint at the bottom of the column, and nodes at the bottom surface were connected to the pivot node accordingly.

After adding the gravity load of 100 kN to the top of the upper column, a displacement history (up to 3.7% drift) was applied to obtain the backbone curve of the subassembly. Lastly, large-deflection effects were included in the analysis. The results from the FE model can be seen in Fig. 2c, along with the experimental curve. The FE model can capture the nonlinear behavior of the subassembly, and the results from the FE model are in good agreement with the experimental data.

$$M(\varphi) = \frac{K\varphi}{\left[1+\left(\frac{K\varphi}{M_{ult}}\right)^{n}\right]^{\frac{1}{n}}} \quad (1)$$

After validating the FE model, different FE models representative of the connections in the structure shown in Fig. 1 were created to calibrate the spring parameters of the VC2. Because beam lengths and axial load vary in each direction and story of the building, six different connections were identified, and their FE models were created to obtain a force-deformation relationship. Then, a simplified model of these connections was developed on OpenSees to calibrate the spring parameters. The calibration progress starts with an assumed set of spring parameters, and then the parameters are adjusted to minimize the difference between numerical results from Ansys and OpenSees. After performing thousands of different analyses on OpenSees, an optimal set of parameters is obtained and listed in Table 2. To achieve faster convergence during this process, rotational stiffness (K) and constant (n) in the power model were fixed to $25E_bI_b/L_b$ and 1.0, respectively, where E_b, I_b, and L_b are elastic modulus, the moment of inertia, and length of the beam, respectively. To illustrate the result, a comparison between the experimental and numerical results for the subassembly is shown in Fig. 2c. In addition, the same connection was modeled with the VC1 to make a fair comparison between VC1 and VC2. As a result, VC1 overestimates the ultimate capacity of the subassembly (i.e., VC2 represents the nonlinear behavior of the subassembly more accurately), and the difference between VC1 and VC2 is more significant at higher drifts.

Table 2. Calibrated Spring Parameters.

Story	Direction	M_{ult} (kNm)	K (kNm/rad)	n
1	X	25.98	11925	1.0
2	X	27.71	11925	1.0
3	X	20.09	11925	1.0
1	Y	24.86	13628	1.0
2	Y	26.59	13628	1.0
3	Y	19.41	13628	1.0

Description of the global models

Two global models, Model 1 and Model 2, were developed on OpenSees to investigate the effect of VC2 on the nonlinear response of the building. Model 1 is basically the same model as previously introduced in Ref. [4]. It has rigid intra-module connections combined with pinned inter-module connections (VC1) for braced and unbraced bays (See Fig. 1d). Model 2, on the other hand, has semi-rigid intra-module connections combined with continuous vertical inter-module connections (VC2) for unbraced bays (See Details B and C in Fig. 1e), and rigid intra-module connections combined with pinned inter-module connections (VC1) for braced bays (See Detail A in Fig. 1e). Because the VC2 was tested and calibrated based on an unbraced configuration, it was only used with unbraced beams and columns. The VC1 was preferred for braced beams and columns. Both models have the same HC. The foundation to module connectivity is provided with a pin connection in both models. As reported by Fathieh and Mercan [4], separate rigid diaphragms are defined at each story to realistically represent the stiffness of the MSB and capture relative displacements and rotations of the modules.

NONLINEAR ANALYSIS

Nonlinear dynamic (time history) analyses were performed to assess the lateral performance of Model 1 and Model 2. The analyses were conducted under the most critical hazard level (Maximum Credible Earthquake (MCE) - associated probability of exceedance per annum 0.404/1000) and the factored gravity loads (1.05D + 0.25L). Twelve pairs of ground motions were selected from the previous study [4], downloaded from the PEER ground motion database [18]. The ground motion records were scaled to the target spectra of the MCE hazard level. The intensity-based assessment of FEMA P58 [19] was used to scale the ground motions. Prior to scaling, a visual assessment is conducted to determine the suitability of the selected ground motion spectra for the target spectrum. This is accomplished by establishing the lower and upper boundaries, based on the minimum value ($T_{min} = 0.2\min(T_{x,1}, T_{y,1})$) and maximum value ($T_{max} = 2.0\max(T_{x,1}, T_{y,1})$) of the fundamental period of the building in the X- and Y-directions ($T_{x,1}$ and $T_{y,1}$). Upon evaluation, it is determined that all ground motions are suitable for the target spectrum. Then the ground motion pairs underwent an amplitude scaling process using a ratio of Sa(T), where T represents the average value of the first modes in both orthogonal directions. The list of ground motion properties, including magnitude, distance to

the fault rupture (R_{rup}), and the scaling factors, are presented in Table 3. The target acceleration spectra, the scaled ground motion spectra, and the geomean of the twelve pairs of records together with T, T_{min}, and T_{max} of the MSB are shown in Fig. 3. As geometric nonlinearity accounted for bracing elements with corotational transformation, P-Delta effects were considered for all beams, columns, and connection elements. 3% Rayleigh damping was assigned to the mass and stiffness matrices using first and third eigenvalues. Additionally, 30 seconds of analysis time (free vibration) was added to the end of each time history analysis to allow the structure to reach a steady state.

Table 3. Ground motion (GM) records and scale factors (SF).

GM #	Record #	Station Name	Year	Magnitude	R_{rup}	SF (MCE)
01	RSN165	Chihuahua	1979	6.53	7.29	1.28
02	RSN176	El Centro Array #13	1979	6.53	21.98	4.07
03	RSN188	Plaster City	1979	6.53	30.33	11.62
04	RSN209	Westmorland Fire Sta	1979	5.62	9.76	5.57
05	RSN729	Superstition Hills-02	1987	6.54	23.85	2.39
06	RSN737	Agnews State Hospital	1989	6.93	24.57	3.35
07	RSN739	Anderson Dam (Downstream)	1989	6.93	20.26	1.44
08	RSN755	Coyote Lake Dam – Southwest Abutment	1989	6.93	20.34	1.47
09	RSN776	Hollister – South & Pine	1989	6.93	27.93	1.04
10	RSN778	Hollister Differential Array	1989	6.93	24.82	1.10
11	RSN806	Sunnyvale – Colton Ave.	1989	6.93	24.23	2.06
12	RSN811	WAHO	1989	6.93	17.47	1.33

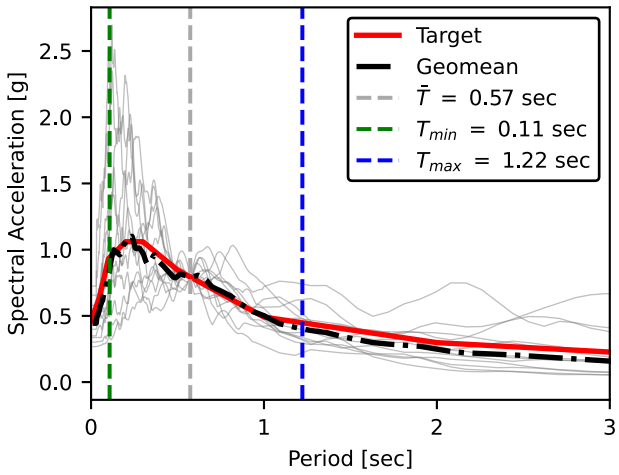

Figure 3. Ground motion scaling.

RESULTS, COMPARISON, AND DISCUSSION

In this section, the results of nonlinear time history analyses (NLTHA) are presented and compared between Model 1 and 2, with a specific emphasis on critical parameters that are indicative of structural behavior during seismic events. Specifically, the base shear, transient and residual inter-story drifts, and hinge formation sequence are examined, as they are critical measures of structural response and can provide insights into a structure's seismic response.

Base shear

Following each analysis, the highest base shears in each perpendicular direction were determined and used to calculate the mean base shear. Figs. 4a and b depict the maximum base shear values in the X- and Y-direction. The average base shear was calculated for both directions and displayed as a solid black line on the figure. In addition, a red line was added to the Figures to indicate if the demand exceeded the yield base shear, which was determined from the pushover analysis that reveals the start of yielding on the diagonal braces.

As shown in Figs. 4a and b, two-thirds of the time histories exceeded the yield limit in the X-direction for Model 1 and 2; however, only one-sixth of records exceeded the yield limit in the Y-direction for both models. In addition, the average base shear exceeded the yield base shear by about 8.5% for both models in the X-direction. Nevertheless, it remained under the yield base shear by 11% for both models in the Y-direction. The highest difference between Model 1 and 2 was observed as 22 kN in GM# 09 in the X-direction.

Moreover, it was found that higher base shear was observed in half of the cases (GM# 01-03, 05, 07, and 08) for Model 2 in the X-direction. For the Y-direction, the highest difference between Model 1 and 2 occurred in GM# 08 by 18 kN. Also, lower base shear was recorded in eleven of the time histories for Model 2 than Model 1. In summary, the results are close to each other, and the difference is insignificant.

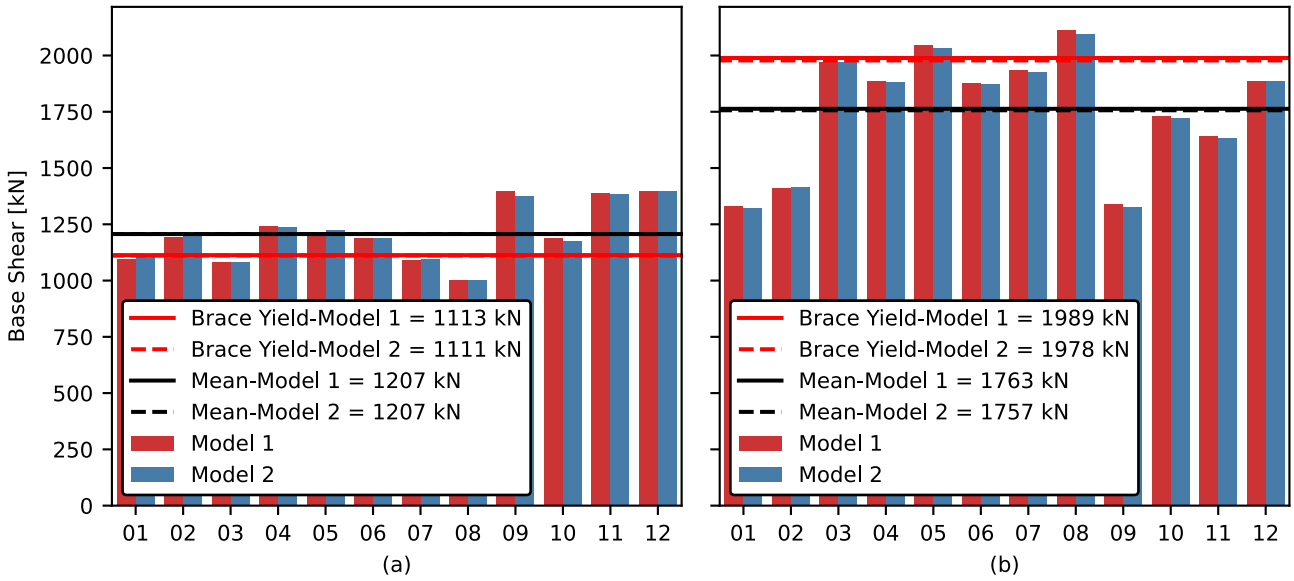

Figure 4. Base Shear Comparison: (a) X-direction and (b) Y-direction.

Inter-story drift ratio

The absolute maximum and residual inter-story drift (IDR) ratios obtained from the NLTHA are another criterion used to compare the dynamic performances of Model 1 and 2. The limit states from FEMA P695 [20] are displayed in Fig. 5 to identify the intensity of the ground motions. 0.5% IDR corresponds to immediate occupancy, 1.5% to life safety, and 2% to collapse prevention. As previously mentioned, yield demand exceeded in the X-direction more than in the Y-direction for both models. Therefore, it is expected to observe higher IDR in the X-direction than in the Y-direction. This is confirmed by the results shown in Figs. 5a. The average maximum transient IDR in the X-direction is close to the life safety limit states with 1.40% and 1.38% for Model 1 and 2, respectively. In addition, both models have exceeded the collapse prevention limit state twice (GM# 09 and 12). Overall, similar performances for both models regarding transient IDR were observed, as depicted in Figs. 5a and b. For example, 0.02% higher transient IDR was recorded for Model 2 than Model 1 in the second story in the X-direction. Besides, a 0.05% higher drift was recorded for Model 1 than Model 2 in the first inter-module connection in the Y-direction.

The residual IDR results are shown in Figs. 5c and d. These values were obtained 30 seconds after each time history. The damage states from FEMA 58 [19] were included in both Figures to give an idea about the damage after each ground motion. The first damage state (DS1) is 0.02% IDR for minor damage, and no alignment is necessary for structural stability. The second damage state is 0.05% IDR for moderate damage, and realignment of the structural frame is required. As can be seen from Figs. 5c and d, the maximum and average residual IDR values are lower than DS1. Even though no significant difference was observed, residual IDRs in Model 2 were consistently higher than in Model 1 in the X-direction. It is also true for the Y-direction except for the second and fourth floor levels. The highest difference between Model 1 and 2 was observed as 0.0057% in the second story in the X-direction and 0.0016% in the fourth story in the Y-direction.

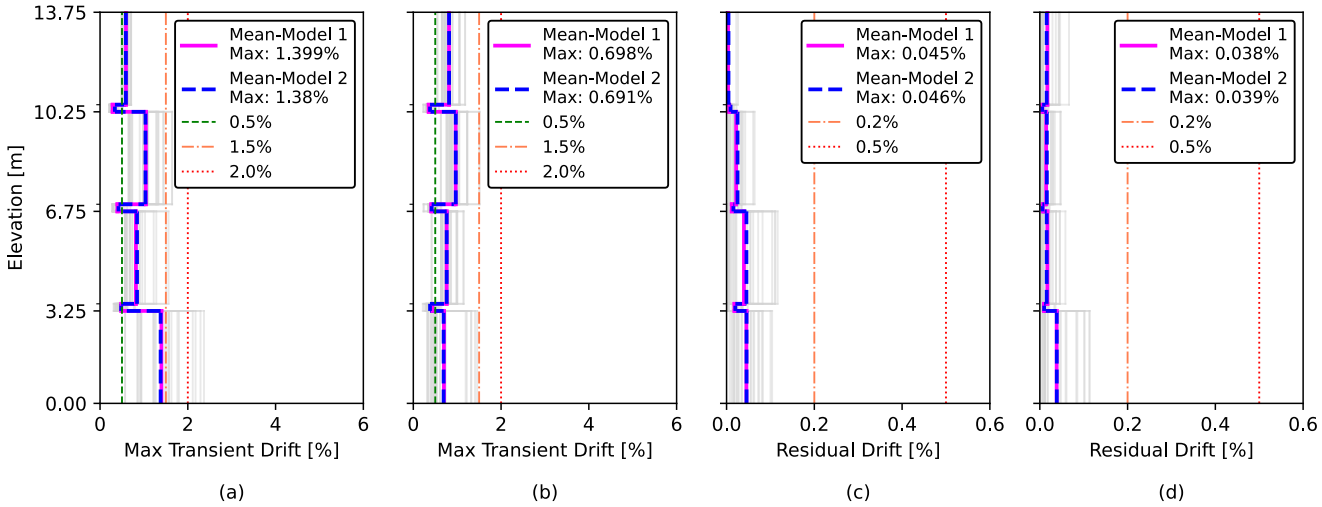

Figure 5. Transient and Residual IDR Comparison: (a) X-direction and (b) Y-direction, (c) X-direction and (d) Y-direction.

Hinge formation sequence

The hinge formation sequence was investigated to determine the effects of VC1 and VC2 on the global dynamic response of the MSB. Fathieh and Mercan [4] reported that inelasticity is mainly concentrated in the first story of the MSB. Thus, the displacement histories of the first story of the MSB for selected ground motions are plotted in Figs. 6 and 7 for the X- and Y-direction, respectively.

As indicated in Figs. 6 and 7, braces started yielding simultaneously for Model 1 and 2 when the building exceeded the immediate occupancy limit state. However, a 3.5% higher transient IDR was recorded in Model 1 than in Model 2 in the X-direction though residual IDRs are identical for both models. It indicates that further investigation might be needed to understand the nonlinear behavior of Model 1 and 2.

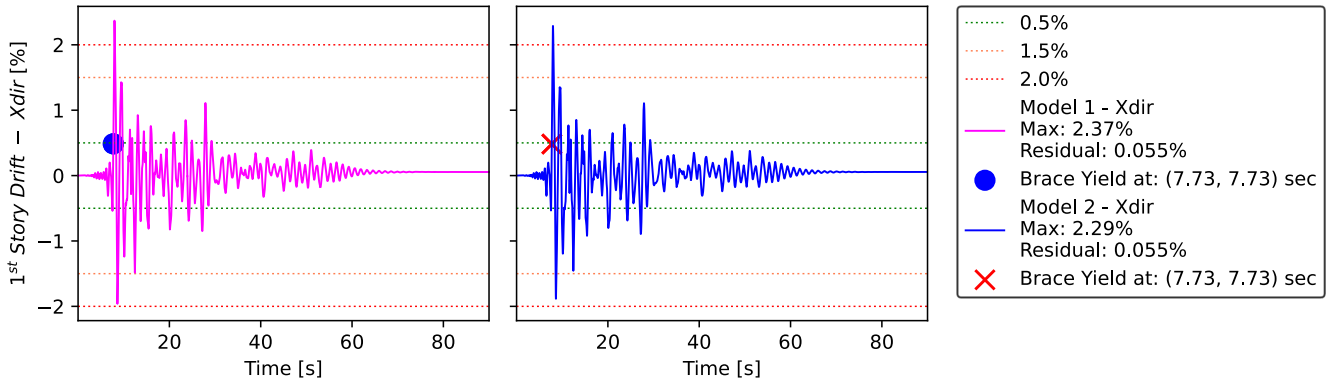

Figure 6. Displacement History of 1st Story of the Building in X-direction for GM09: (left) Model 1 and (right) Model 2.

CONCLUSIONS

This paper investigates the effect of modeling welded vertical inter-module connections on the nonlinear dynamic response of a low-rise MSB. Initially, two different welded vertical inter-module connection models in the literature were identified. Subsequently, detailed FE models were developed to obtain the parameters of one of the connection models. Afterward, both connection models were integrated into global models of the MSB, which were modeled in 3-D using OpenSees. Finally, bidirectional nonlinear time history analyses were performed to evaluate the seismic performance of two global models. Base shears values, transient and residual inter-story drifts, and hinge formation in the braces were discussed in detail. Key findings are summarized below:

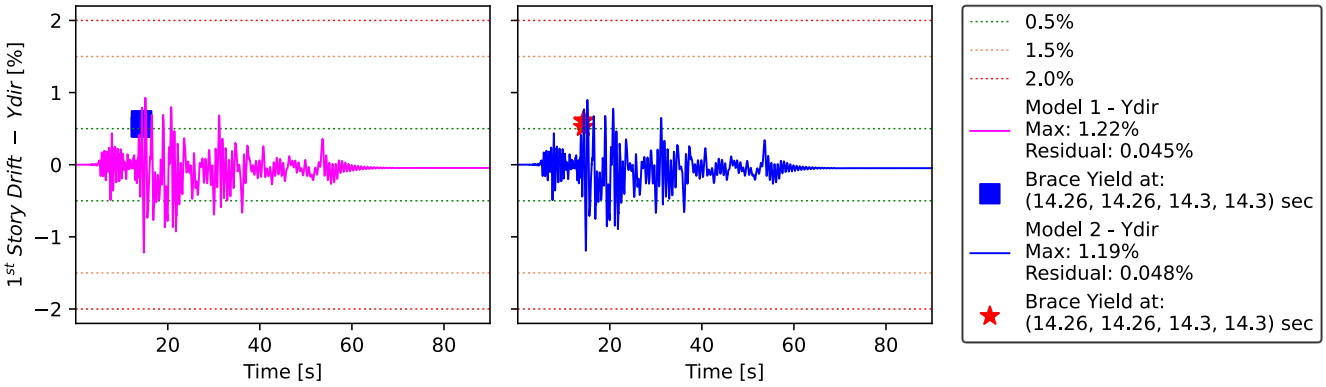

Figure 7. Displacement History of 1st Story of the Building in Y-direction for GM05: (left) Model 1 and (right) Model 2.

1. Base shear values of the two global models were similar, and the difference was about 1% of the average base shear in the X- and Y-direction.
2. IDR results showed that VC2 could cause slight differences in the transient and residual IDR. However, the difference is more pronounced in the residual IDRs.
3. Although the braces in both models yielded simultaneously, further research is recommended to understand the distribution of nonlinearity among the structural members since differences in the maximum transient IDR were observed.

While this study demonstrates that a more detailed modeling of the welded vertical inter-module connection (VC2) has no significant impact on the response of a low-rise MSB, further research is recommended for mid- and high-rise MSBs.

ACKNOWLEDGMENTS

This paper is based upon work funded by the Natural Sciences and Engineering Research Council of Canada (NSERC) Discovery (202205127) Program and funding from Erwin Edward Hart Professorship. Computations were performed on the Niagara and Graham supercomputers of the Digital Research Alliance of Canada. The authors would like to thank Rafaela Sanches for their contributions and to SHARCNET for providing Ansys licenses for academic use. Any opinions, findings, conclusions, and recommendations expressed here are those of the authors and do not necessarily reflect the views of the sponsors.

REFERENCES

[1] M. Lawson, R. Ogden, C. Goodier, Design in Modular Construction, Taylor & Francis Group, LLC, 6000 Broken Sound Parkway NW, Suite 300 Boca Raton, FL 33487-2742, 2014.
[2] M. T. Gorgolewski, P. J. Grubb, R. M. Lawson, C. Mice, Design of Residential Buildings (2009).
[3] C. Annan, M. Youssef, M. El Naggar, Experimental evaluation of the seismic performance of modular steel-braced frames, Engineering Structures 31 (7) (2009) 1435–1446. doi:https://doi.org/10.1016/j.engstruct.2009.02.024.
[4] A. Fathieh, O. Mercan, Seismic evaluation of modular steel buildings, Engineering Structures 122 (2016) 83–92. doi: https://doi.org/10.1016/j.engstruct.2016.04.054.
[5] S. Srisangeerthanan, M. J. Hashemi, P. Rajeev, E. Gad, S. Fernando, Review of performance requirements for inter-module connections in multi-story modular buildings, Journal of Building Engineering 28 (2020) 101087. doi:https://doi.org/10.1016/j.jobe.2019.101087.
[6] A. W. Lacey, W. Chen, H. Hao, K. Bi, Effect of inter-module connection stiffness on structural response of a modular steel building subjected to wind and earthquake load, Engineering Structures 213 (2020) 110628. doi:https://doi.org/10.1016/j.engstruct.2020.110628.
[7] R. Sanches, O. Mercan, B. Roberts, Experimental investigations of vertical post-tensioned connection for modular steel structures, Engineering Structures 175 (2018) 776–789. doi:https://doi.org/10.1016/j.engstruct.2018.08.049.
[8] R. Sanches, Development of vertical post-tensioned connection for modular steel buildings, Ph.D. thesis, University of Toronto (2022).
[9] Ansys Inc, Ansys® Academic Research Mechanical, Ansys Software v22.2. Ansys Inc., Canonsburg, PA, USA. (2022). URL https://www.ansys.com/

[10] M. Zhu, F. McKenna, M. H. Scott, Openseespy: Python library for the opensees finite element framework, SoftwareX 7 (2018) 6–11. doi: https://doi.org/10.1016/j.softx.2017.10.009
[11] NBCC, National Building Code of Canada, Institute for Research in Construction, National Research Council of Canada, Ottawa, Ontario, 2010.
[12] D. G. Lignos, H. Krawinkler, Deterioration modeling of steel components in support of collapse prediction of steel moment frames under earthquake loading, Journal of Structural Engineering 137 (11) (2011) 1291–1302. doi: https://doi.org/10.1061/(ASCE)ST.1943-541X.0000376.
[13] D. Lignos, Sidesway collapse of deteriorating structural systems under seismic excitations, Ph.D. thesis, Stanford University (2008).
[14] P.-C. Hsiao, D. E. Lehman, C. W. Roeder, Improved analytical model for special concentrically braced frames, Journal of Constructional Steel Research 73 (2012) 80–94. doi:https://doi.org/10.1016/j.jcsr.2012.01.010.
[15] A. Colson, J. M. Louveau, Connections incidence on the inelastic behavior of steel structures, Euromech Colloguium 174 (1983).
[16] A. Kaszynski, pyansys: Python Interface to MAPDL and Associated Binary and ASCII Files (2020). doi: https://doi.org/10.5281/zenodo.4009467.
[17] X.-D. Bu, Irregular welded rectangular hollow section truss-type connections, Ph.D. thesis, University of Toronto (2022).
[18] PEER Ground Motion Database, available online: https://ngawest2.berkeley.edu (accessed on January 23, 2023).
[19] FEMA P-58, Seismic Performance Assessment of Buildings, Volume 2 – Methodology, Second Edition, Federal Emergency Management Agency, Washington, DC, 2018.
[20] FEMA P695, Quantification of Building Seismic Performance Factors, Federal Emergency Management Agency, Washington, DC.